24th International Conference on Renewable Energies and Power Quality (ICREPQ'26)
Santander (Spain), 10th to 12th June 2026
ISBN-13: 978-84-09-82044-3

Physical Model Experimental Study on Tidal Current Turbines Development in Narrow Channels

Qingjun Li, Hongwei Liu ,Kun Zhou

The State Key Laboratory of Fluid Power and Mechatronic Systems,
Zhejiang University, Hangzhou 310027, China.
Qingjun98@zju.edu.cn

Abstract. To investigate the flow field and energy extraction characteristics of tidal current turbine array deployment in narrow channels, this study established a physical model experimental system based on a circulating pool. Three turbine configurations with distinct transmission systems and a high-performance rotor optimized for low-velocity conditions were developed, with narrow channel conditions simulated using flow baffles. Through observation and analysis of the energy capture and channel flow variations of single, dual, and quadruple turbine arrays, this study ultimately reveals, at a macroscopic level, the relationship between dynamic inflow and turbine operating states, and at a microscopic level, the relationship between flow field reconstruction and power capture characteristics, thereby providing experimental evidence for optimized array layout and engineering applications.

Key words. Tidal current turbine, Array development, Experimental study, Dynamic inflow,Narrow channel

1. Introduction

Narrow channels, due to their unique topography, generate strong currents with significantly higher energy concentration compared to open seas, making them the primary target for large-scale tidal energy development [1]. The key approach to efficiently utilizing resources in these areas is the deployment of large tidal current turbine arrays [2]. However, array deployment is constrained by complex hydrodynamic interactions at both farm-wide and local levels [3]. At the farm scale, the array configuration modifies the ambient channel flow, thereby influencing the total extractable energy. Conversely, at the turbine scale, local flow restructuring under multi-boundary conditions may accelerate flow, potentially enhancing the power output of downstream turbines. Based on tidal dynamics theory, Garrett [4][5] proposed that the maximum extractable energy from an ideal tidal channel is approximately 22% of the undisturbed flow energy, and boundary effects can increase the turbine power coefficient by a factor of $(1-A/Ac)^{-2}$. Vennell et al.[6] further indicated that under conditions of high blockage ratio and an optimized layout, array turbines can exceed the Betz limit, with individual turbines outperforming their isolated operation even when the overall channel flow is reduced. While these theories provide macro-level guidance for array development, current research has not experimentally quantified the relationship between turbine performance parameters and the dynamic balance of channel flow, a critical bottleneck for engineering applications.

Current experimental research on tidal energy turbine arrays primarily focuses on characterizing turbine wake fields through systematic observation, to elucidate the underlying correlations between wake dynamics and turbine performance metrics, thereby informing evidence-based recommendations for optimized array configuration and spatial layout. For instance, Chen et al.[7][8] investigated the three-dimensional wake structures of tidal turbines in flume experiments, revealing that significant velocity deficits with limited diffusion characterize the near-wake region. In contrast, the far-wake region exhibits gradual velocity recovery and enhanced turbulent spreading. Based on these observations, they recommended optimal array configurations with lateral spacing >1.5D, longitudinal spacing >5D, and staggered inter-row spacing <12D to balance power output and mitigate wake interference. Similarly, Zhang et al. [9]conducted experiments with a four-turbine array in a circulating water tank and proposed a layout reference of 1.5D lateral and 5D longitudinal spacing. Mycek et al.[10][11] found that high turbulence intensity can accelerate wake recovery, thereby improving downstream turbine performance. In their follow-up research, Gaurier et al. [12] demonstrated that turbine layout configuration exerts a significant influence on wake characteristics and performance metrics, with downstream turbines achieving enhanced power output under appropriately optimized environmental conditions and spatial arrangements. Nuremberg ' s [13] PIV observations indicated that staggered arrangements optimize wake recovery, with a 15% velocity deficit still present at a longitudinal distance of 20D. Stallard [14] noted that wake merging occurs when the lateral spacing is less than 2D. However, these studies exhibit three main limitations: first, the experimental rotors are often scaled models of large blades, making it difficult to guarantee the power coefficient under low-flow conditions; second, many experiments are conducted under low blockage ratios, failing to capture the high-speed lateral flow effects caused by rotor blockage at high blockage ratios; third, some experiments use motor-driven rotors instead of actual energy capture modes, which cannot accurately reflect the hydrodynamics-power coupling characteristics. Consequently, while existing research has clarified wake evolution patterns, it has not revealed the dynamic balance mechanism of channel flow induced by turbine arrays in large-scale development or the effects of multi-boundary flow-field reconstruction. There is an urgent need to fill this gap through physical model experiments.

This study established a high-fidelity experimental system for a physical model based on a circulating flume. The experimental framework comprises three pivotal components: first, the physical emulation of a nearshore narrow-channel environment via flow-confinement structures; second, the development of a high-performance rotor optimized for low-velocity regimes; and third, the investigation of resource-development characteristics associated with diverse turbine-layout configurations within such a narrow channel.

2. Experimental setup

A. Low-velocity rotor design

Based on the NACA63412 airfoil profile, a low-velocity rotor was designed(Fig. 1), and their hydrodynamic performance was analyzed using CFD simulations. The rotor was fabricated as a monolithic structure using stereolithography (SLA) with a photosensitive resin. To enhance mechanical strength, the blade surfaces were coated with a fiberglass-reinforced composite layer. The rotor parameters are shown in Tab. 1.

Fig. 1. Rotor designed for low-velocity conditions

Tab. 1. Low-velocity rotor parameters

Parameter	Symbol	Value
Rotor diameter(m)	D	0.7
Hub radius(m)	R_{hub}	0.03
Rated inflow velocity(m/s)	v_{rated}	0.8
Rated rotational speed(rpm)	ω_{rated}	87.3
Optimal tip speed ratio	λ_{opt}	4.0
Number of blades	n	3
Optimal power coefficient	C_{Popt}	0.43

The Tip Speed Ratio (TSR) is the fundamental parameter used to describe rotor performance, defined as the ratio of the rotor tip velocity to the upstream flow velocity.

$$TSR = \frac{|\Omega| R}{U_\infty} \tag{1}$$

where Ω is the rotor angular velocity about its central axis (rad/s), R is the rotor radius (m), and U_∞ is the upstream flow velocity (m/s). In our study, the turbine TSR varies from 1.5 to 7.5. At the optimal tip-speed ratio of 4, the rotor exhibits its peak power coefficient (C_P).

The power coefficient serves as a key performance metric for converting the hydraulic energy $E_{hydraulic}$ available in the flow.C_P is defined as the proportion of power P retrieved by the turbine as compared to the maximum available power P_∞ from the incoming flow through the rotor area A.

$$C_P = \frac{P}{P_\infty} = \frac{T\Omega}{\frac{1}{2}\rho A U_\infty^3} = \frac{T\Omega}{\frac{1}{2}\rho \pi R^2 U_\infty^3} \tag{2}$$

where T is the torque on the rotor about its central axis (N·m), ρ is the density of the fluid (kg/m³). The mechanical energy of the rotor is converted into electrical energy E_{out} by the generator after passing through the drive train. In this study, two distinct methods were employed to measure the power acquired by the turbine. The first method involved direct measurement using a torque sensor. The second method indirectly determined the power based on the generator's output voltage and current, together with the turbine's electromechanical conversion efficiency η_{m-e}. A formula can express the energy transfer process.

$$E_{out} = E_{hydraulic} * C_P * \eta_{m-e} \tag{3}$$

To obtain this electromechanical efficiency, a drag test was specifically designed and conducted.

$$B_r = \frac{A_R}{A_C} \tag{4}$$

B_r represents the blockage ratio, where A_R is the projected area of the rotor, and A_C is the cross-sectional area of the channel. A high blockage ratio condition is considered to occur when $B_r > 0.1$.

The flow loss ratio, Bloss, is defined as the ratio of the flow rate lost in the channel, Q_L, due to the presence of turbines, to the flow rate, Q_0, in the absence of turbines.

$$B_{loss} = \frac{Q_L}{Q_0} \tag{5}$$

B. Low-velocity rotor design

In the experiment, four turbines developed in-lab for low-velocity applications were employed (Fig. 2). All four turbine units employ magnetic couplers to achieve contactless transmission between the rotor and the generator. This design avoids frictional losses caused by dynamic seals and effectively reduces energy dissipation[15][16].

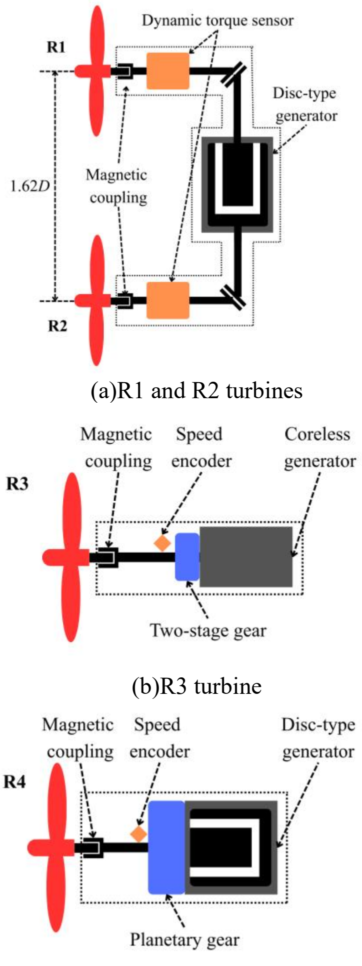

(a)R1 and R2 turbines

(b)R3 turbine

(c)R4 turbine

Fig. 2. The four turbines used in the experiment

To characterize the turbine's electromechanical conversion efficiency, a motor-driven test was performed. Fig. 3 illustrates the test details.The drive motor, equipped with a gear reducer, provided rotational speed n and torque T within the operational range required for the rotor, serving as the energy input for the turbine. A dynamic torque sensor monitored this input. The turbine generator was connected to an adjustable load, R_{load}, and its output voltage, V_{out}, was monitored by an electrical signal acquisition device. The calculation process is as follows.

$$\eta_{m-e} = \frac{V_{out}^2}{R_{load} * nT} \quad (4)$$

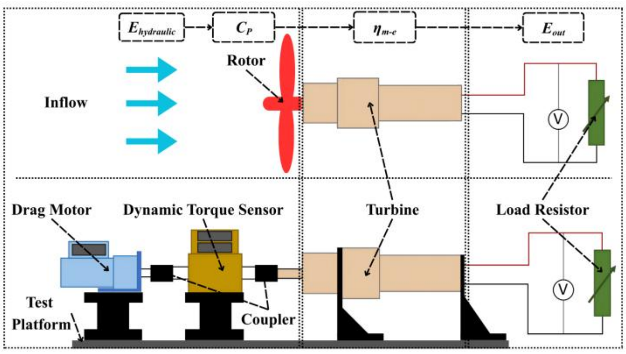

Fig. 3. Motor-driven experiment

C. Experimental environment design

This experiment was conducted in the wave-current coupling flume at the State Key Laboratory of Coastal and Offshore Engineering of Ocean University of China. To simulate the flow field environment in a nearshore narrow channel, blockage panels were employed to replicate the convergence effect of islands or landmasses on the current(Fig. 4). The panels were arranged on the outlet side of the water tank in a fan-shaped configuration with a 90-degree included angle. A partial gap was reserved on the inlet side to simulate the scenario where the current bypasses the island or landform and enters adjacent channels, allowing a portion of the free-stream flow to circumvent the blockage panels.

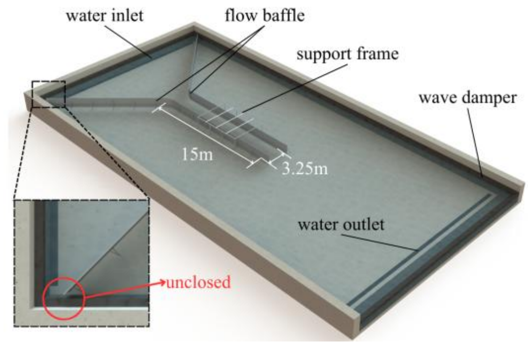

Fig. 4. Narrow channel layout in circulating pool

Flow velocity was measured using an Acoustic Doppler Velocimeter (ADV) and a high-precision Acoustic Doppler Current Profiler (ADCP). The ADV was placed at a 5D upstream location to monitor inflow velocity variations, while the ADCP provided auxiliary monitoring to assess inflow uniformity. Electrical parameter sensors were used to measure the electrical output of each tidal turbine directly. This approach bypasses the complexity of wake monitoring and enables direct measurement of the power-capture performance of individual rotors within the array.

D. Turbines layout

The experimental protocol primarily comprised the following components.The empty channel test was conducted to obtain the flow velocity distribution within the channel in the absence of any tidal turbines, establishing a baseline for assessing the channel's resource potential(Fig. 5.(a)). The single turbine performance test focused on investigating the power capture performance of an isolated unit within the narrow channel and the associated changes in upstream flow velocity(Fig. 5(b)). The performance test of two single turbine units specifically investigated the coupling in energy capture between upstream and downstream units within the channel, with a key analysis on the degree of power capture inhibition imposed on the downstream unit by the upstream unit operating at different tip speed ratios(Fig. 5(c)(d)).The four-turbine array test further examined the coupling relationship between the array layout and power extraction, aiming to inform strategies for efficient channel resource utilization.(Fig. 5(e)(f))

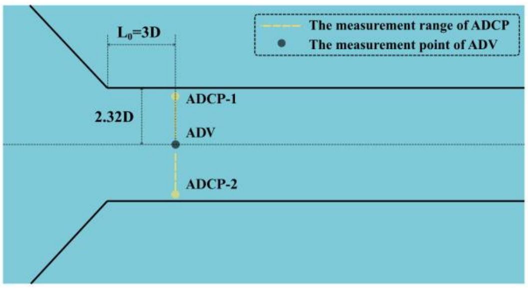

(a)Empty channel

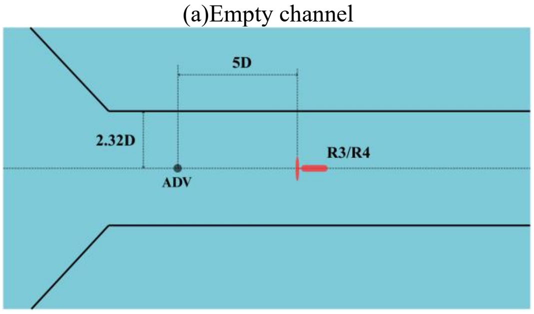

(b)Single turbine

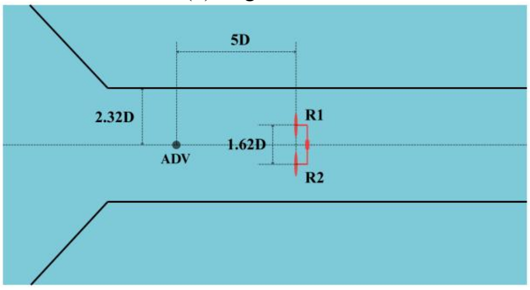

(c)Two turbines arranged in parallel

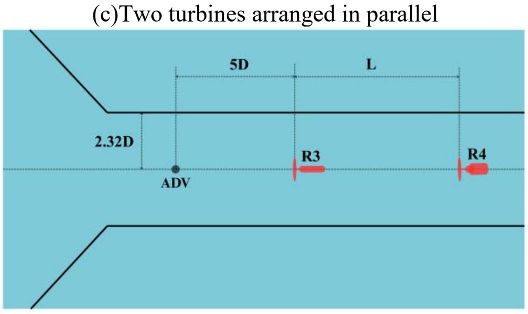

(d)Two turbines arranged in tandem

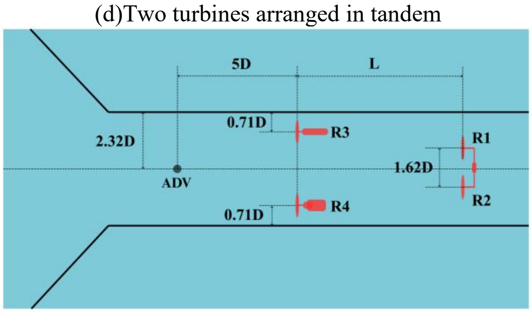

(e)Four-turbine array "2+1."

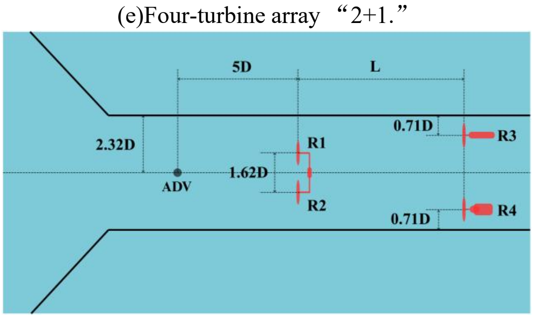

(f)Four-turbine array "1+2."

Fig. 5. Turbines layout in a narrow channel

3. Result and discussion

A. Empty channel

Synchronous recordings were taken at 40 sampling points across the channel cross-section.The average flow velocity was 0.75175m/s with a standard deviation σ of 0.0383m/s, resulting in an ambient turbulence intensity rate I_∞ of approximately 5%.

B. Single-turbine and two turbines arranged in parallel

Tab. 2Performance of turbines(*This value represented the baseline of a single rotor in the narrow channel)

Rotor	Average power capture(W)	Average upstream flow velocity(m/s)	Average power coefficient
R1 (R2)	38.88	0.6961	0.599
R3	43.94*	0.7179	0.605
R4	42.69	0.7123	0.601

By adjusting the load, the turbine operates at its optimal condition. As detailed in Tab. 2., the rotor's efficiency was derived from power performance and flow rate data. The results indicate that while a parallel turbine arrangement reduces the flow rate, the overall energy capture efficiency is maintained.

C. Two turbines arranged in tandem

As shown in the Fig. 6., the comparison of rotational speed and captured power reveals that the optimal operating point of the downstream turbine R4 exhibits a nonlinear response to changes in the TSR of R3. The captured power of R4 shows a gradual decreasing trend, while its corresponding rotational speed first decreases and then increases. The following inferences can be drawn: when the tip-speed ratio of R3 is low, both its energy capture and flow-blocking effects are relatively weak, resulting in a less severe wake deficit and favorable inflow conditions for R4. As the rotational speed of R3 gradually increases to 77 rpm (optimal TSR = 4), its energy capture and blocking effects intensify, leading to a progressively greater wake deficit and a gradual reduction in the inflow velocity at R4. When the rotational speed of R3 further rises to 135 rpm(TSR = 7.3)—at which point its load circuit is disconnected —the wake deficit increases sharply. The higher turbulence intensity in the inflow to R4 further reduces the captured power at spacings of 9D and 12D. However, under these conditions, the rapid destabilization of tip vortices accelerates wake recovery, so the captured power of R4 at 15D no longer exhibits additional attenuation.

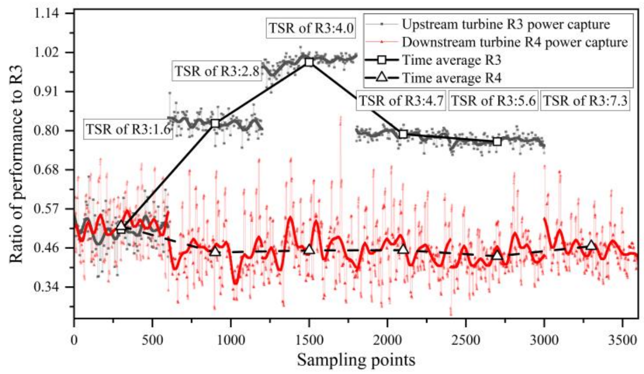

(a)The performance of R3 and R4 when L=9D

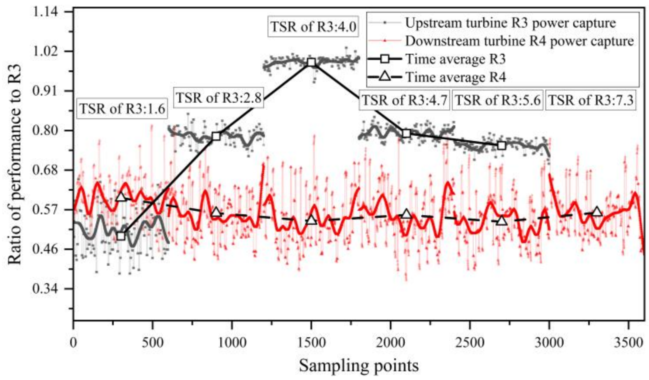

(b)The performance of R3 and R4 when L=12D

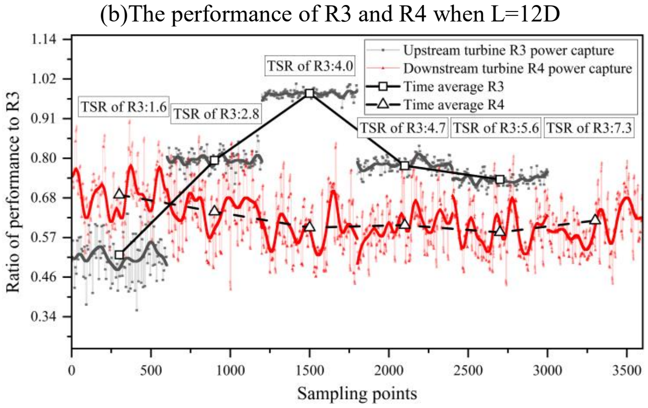

(c)The performance of R3 and R4 when L=15D

Fig. 6. Comparison of performance between R3 and R4
(The vertical coordinate is the ratio to the reference * in Tab. 2.)

D. Four-turbine arrays

Fig. 7. Four-turbine arrays experiment layout

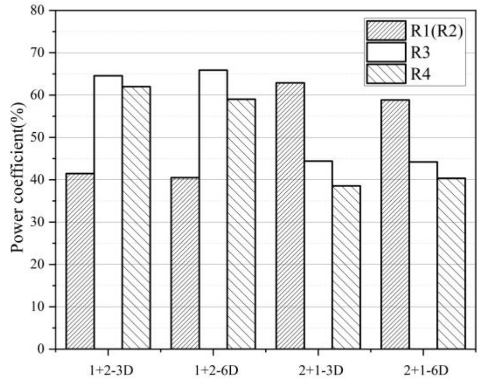

Fig. 8. Comparison of rotor captured power in four-turbine arrays

Fig. 7. illustrates an array of four turbines in a narrow channel. In this configuration, R3 and R4 are arranged in parallel upstream, while R1 and R2 are arranged in parallel downstream. The distance between the upstream and downstream turbines is 3D. This arrangement is hereafter referred to as "2+1-3D".The optimal operating point of the upstream and downstream turbines was adjusted sequentially. Data were recorded synchronously once the flow field stabilized.

The flow rate further decreased to approximately 0.66 m/s. Based on the generator's power output, the energy captured by the rotors was calculated (Fig. 8.). The average power of the downstream unit exceeded that of the upstream unit by 49.4 %, with slightly higher values at L = 3D compared to L = 6D. Both values were substantially greater than the results when the unit operated alone in the channel.From these observations, the following reasonable inferences can be drawn. As the flow passes the upstream unit, a portion of the water bypasses the rotor and accelerates, forming a high-speed lateral flow. This portion of energy can effectively act on the downstream rotor, enhancing its power capture performance. Energy exchange between the high- speed lateral flow and the upstream wake is the main mechanism for wake recovery. At L = 3D, this energy exchange is not yet fully developed, resulting in limited wake recovery, and the inflow to the downstream unit is dominated by high- speed lateral flow. At L = 6D, enhanced mixing between the lateral flow and the wake promotes partial energy exchange, expanding the region influenced by the wake. Under this condition, the inflow to the downstream unit consists of an incompletely recovered wake combined with a portion of high- speed lateral flow.

E. *Discussion*

In narrow channels, an increase in the blockage ratio leads to a reduction in channel flow. In the model constructed in this experiment, the blockage ratio exhibits a positive correlation with flow loss, with the fitted curve showing a slope of approximately 0.22 (Fig. 9.) However, the blockage effect induced by multiple boundaries can significantly enhance the power capture capability of turbines. The power captured by downstream turbines within an array substantially exceeds that of turbines operating in isolation within the same channel. Based on this observation, the following reasonable hypothesis can be made: As the flow passes the upstream turbines, a portion of the water bypasses the rotors and accelerates, forming a high-velocity side flow. This flow, carrying additional kinetic energy, can act effectively on the downstream turbines, thereby improving their power capture performance. Furthermore, the energy exchange between this high-velocity side flow and the upstream wake is likely a primary mechanism contributing to wake recovery.

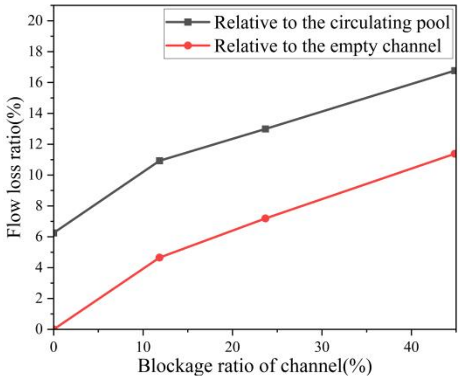

Fig. 9. Blocking ratio causes flow loss

4. Conclusion

This experimental study demonstrates that the blockage effect induced by the turbines themselves significantly influences the exploitation of tidal current energy in constrained waterways. First, within the experimentally constructed narrow-channel model, a positive correlation was observed between the blockage ratio and the flow loss ratio: specifically, each 1% increment in blockage ratio corresponded to an average increase of 0.22% in flow loss. Furthermore, no significant correlation was observed between TSR and flow loss, with the latter exhibiting low sensitivity to variations in TSR.

However, in staggered turbine arrays deployed within the narrow channel, an overall trend emerged wherein energy capture diminished for upstream units while increasing for downstream units; in this experiment, downstream turbines harvested, on average, 49.4% more energy than their upstream counterparts. This finding suggests that, under multi-boundary conditions, while turbines impede flow and induce discharge losses, they also modify the local flow-field structure. Such modifications accelerate flow velocities between boundaries, thereby conferring a performance advantage to downstream turbines.

This paper provides effective support for the development of tidal turbine arrays. Under reasonable layout and parameter matching, the tidal energy resources in narrow channels can achieve efficient and intensive utilization. It offers valuable design references for subsequent engineering applications.

Acknowledgement

This work was supported by the National Key R&D Program of China(2023YFB4204102).

References

[1] Vennell, Ross, et al. "Designing large arrays of tidal turbines: A synthesis and review." Renewable and Sustainable Energy Reviews 41 (2015): 454-472.

[2] Garrett, Chris, and Patrick Cummins. "The power potential of tidal currents in channels." Proceedings of the royal society A: mathematical, physical and engineering sciences 461.2060 (2005): 2563-2572.

[3] Garrett, Chris, and Patrick Cummins. "The efficiency of a turbine in a tidal channel." Journal of fluid mechanics 588 (2007): 243-251.

[4] Garrett, C., Cummins, P., 2005. The power potential of tidal currents in channels. Proc. R. Soc. A. 461, 2563–2572.

[5] Garrett, C., Cummins, P. (2007. The efficiency of a turbine in a tidal channel. J. Fluid Mech. 588, 243–251.

[6] Vennell, R., 2013. Exceeding the Betz limit with tidal turbines. Renewable Energy 55, 277–285.

[7] Chen, Y., Lin, B., Lin, J., Wang, S., 2017. Experimental study of wake structure behind a horizontal axis tidal stream turbine. Applied Energy 196, 82–96.

[8] Chen, Y., Sun, J., Lin, B., Lin, J., Guo, J., 2021. Spatial evolution and kinetic energy restoration in the wake zone behind a tidal turbine: An experimental study. Ocean Engineering 228, 108920.

[9] Zhang, J., Wang, G., Lin, X., Zhou, Y., Wang, R., Chen, H., 2023. Experimental investigation of wake and thrust characteristics of a small-scale tidal stream turbine array. Ocean Engineering 283, 115038.

[10] Mycek, P., Gaurier, B., Germain, G., Pinon, G., Rivoalen, E., 2014. Experimental study of the turbulence intensity effects on the behaviour of marine current turbines. Part I: One single turbine. Renewable Energy 66, 729–746.

[11] Mycek, P., Gaurier, B., Germain, G., Pinon, G., Rivoalen, E., 2014. Experimental study of the turbulence intensity effects on marine current turbines behaviour. Part II: Two interacting turbines. Renewable Energy 68, 876–892.

[12] Gaurier, B., Carlier, C., Germain, G., Pinon, G., Rivoalen, E., 2020. Three tidal turbines in interaction: An experimental study of turbulence intensity effects on wakes and turbine performance. Renewable Energy 148, 1150–1164.

[13] Nürnberg, M., Tao, L., 2018. Experimental study of wake characteristics in tidal turbine arrays. Renewable Energy 127, 168–181.

[14] Stallard, T., Collings, R., Feng, T., Whelan, J., 2013. Interactions between tidal turbine wakes: experimental study of a group of three-bladed rotors. Phil. Trans. R. Soc. A. 371, 20120159.

[15] Liu, H., Fang, J., Gu, Y., Gao, Z., Feng, X., 2024. Design and tests of a marine current turbine in low flow velocity. Ocean Engineering 313, 119595.

[16] Liu, H., Li, H., Gu, Y., Ding, K., Lin, Y., Lou, L., Li, R., Fang, L., 2025. High-efficiency twin-rotor direct-drive marine current turbine: Design, tests, and performance evaluation. Energy 329, 136691.